Acta Crystallographica Section B
Structural Science
ISSN 0108-7681

X-ray powder diffraction and electron diffraction studies of the thortveitite-related *L* phase, $(Zn,Mn)_2V_2O_7$

Kevin M. Knowles,[a]* Mary E. Vickers,[a] Anjan Sil,[b] Yung-Hoe Han[a] and Périne Jaffrenou[a]‡

[a]Department of Materials Science and Metallurgy, University of Cambridge, Pembroke Street, Cambridge CB2 3QZ, England, and [b]Department of Metallurgical and Materials Engineering, Indian Institute of Technology Roorkee, Roorkee 247 667, Uttarakhand, India

‡ Current address: Laboratoire d'Etude des Microstructures, ONERA-CNRS, Boîte Postale 72, 92322 Châtillon CEDEX, France

Correspondence e-mail: kmk10@cam.ac.uk

Received 10 November 2008
Accepted 12 December 2008

The phase designated γ-$Zn_3(VO_4)_2$ reported as a minor second phase in zinc oxide-based varistor materials doped with vanadium oxide and manganese oxide is shown to be the *L* phase, $(Zn_{1-x}Mn_x)_2V_2O_7$ ($0.188 < x < 0.538$), in the pseudo-binary $Mn_2V_2O_7$–$Zn_2V_2O_7$ system. Analysis of X-ray powder diffraction patterns and electron diffraction patterns of this phase shows that the previously published *a*, *c* and β values for this thortveitite-related phase are incorrect. Instead, Rietveld refinement of the X-ray powder pattern of the *L* phase shows that it has a monoclinic *C* lattice with $Z = 6$, with $a = 10.3791\ (1)$, $b = 8.5557\ (1)$, $c = 9.3539\ (1)$ Å and $\beta = 98.467\ (1)^\circ$. Although prior convergent-beam electron diffraction work of 'γ-$Zn_3(VO_4)_2$' confirmed the *C* Bravais lattice, the space group was found to be *Cm* rather than *C*2/*m*, the difference perhaps arising from the inability of the X-rays to detect small displacements of oxygen. Attempts to refine the structure in *Cm* did not produce improved *R* factors. The relationship between the crystal structure of the *L* phase and the high-temperature *C*2/*m* β'-$Zn_2V_2O_7$ thortveitite-type solid solution is discussed.

1. Introduction

Recent work on zinc oxide varistor materials where small amounts of manganese oxide and vanadium oxide are typically added at levels of up to 2 mol% have shown that technologically useful varistors with non-linear current-voltage coefficients in excess of 20 can be readily produced (Kuo *et al.*, 1998; Hng & Knowles, 2000; Hng & Chan, 2002, 2004; Chen, 2003; Pfeiffer & Knowles, 2004; Nahm, 2007*a*,*b*; Nahm, 2008*a*,*b*). The advantage of such varistors is that they can be sintered successfully at temperatures around 1173 K, significantly lower than current commercial multi-oxide varistor formulations containing either bismuth oxide or praseodymium oxide (Hng & Knowles, 2000).

The microstructure of these varistor materials based on zinc oxide with additions of manganese oxide and vanadium oxide consists of zinc oxide grains, typically of the order of 5–10 μm grain size and doped with manganese, vanadium-rich zinc oxide grain boundaries, and small sub-μm-sized second-phase particles located at grain boundaries and triple junctions (Hng & Knowles, 2000; Pfeiffer & Knowles, 2004). Energy-dispersive X-ray microanalysis of these second-phase particles has shown that they contain zinc, manganese and vanadium, with a (Zn + Mn):V ratio of approximately 1:1 within experimental error (Hng *et al.*, 2001). Ignoring the oxygen present in these particles, the relative atomic percentages of zinc, manganese and vanadium have been quoted as being 39.2 at% zinc, 13.8 at% manganese and 47 at% vanadium (Hng *et al.*, 2001).

These particles have been designated γ-$Zn_3(VO_4)_2$ by a number of workers from the identification of a few relatively weak peaks just above the background in powder X-ray diffraction patterns of the sintered varistor formulations (Hng & Knowles, 2000; Hng & Chan, 2002, 2004; Chen, 2003; Pfeiffer & Knowles, 2004). However, as Hng *et al.* (2001) have discussed, it is entirely possible that this phase is not the phase identified by Brown & Hummel (1965) in their examination of chemical reactions between zinc oxide and selected elements of Groups I and V, and labelled γ-$Zn_3(VO_4)_2$, but is instead a completely different compound composed of zinc, manganese, vanadium and oxygen. The present investigation shows that this is indeed the case, and that 'γ-$Zn_3(VO_4)_2$' is in fact the *L* phase reported in the pseudobinary $Mn_2V_2O_7$–$Zn_2V_2O_7$ system. This work has also been able to produce a model of the crystal structure of the *L* phase through Rietveld refinement of laboratory X-ray powder diffractometry data.

2. Phase equilibria and crystal structure considerations

The recent reassessment of phase equilibria in the V_2O_5—ZnO system by Kurzawa *et al.* (2001) found no evidence for the occurrence of γ-$Zn_3(VO_4)_2$. Instead, Kurzawa and co-workers showed that $Zn_3(VO_4)_2$ does not exhibit the polymorphism suggested by Brown & Hummel (1965), only occurring as the phase labelled α-$Zn_3(VO_4)_2$ by Brown & Hummel. α-$Zn_3(VO_4)_2$ is known to crystallize with an orthorhombic *Cmca* structure (Gopal & Calvo, 1971), in contrast to the phase labelled γ-$Zn_3(VO_4)_2$ in zinc oxide varistor formulations which has been shown from an analysis of electron diffraction patterns to have a monoclinic *C* lattice with $a = 10.40$, $b = 8.59$, $c = 9.44$ Å and $\beta = 98.8^\circ$ (Hng & Knowles, 1999). Convergent-beam electron diffraction (CBED) analysis at and around the [100] and [001] axes of this phase has shown further that its space group is *Cm* (Hng *et al.*, 2001).

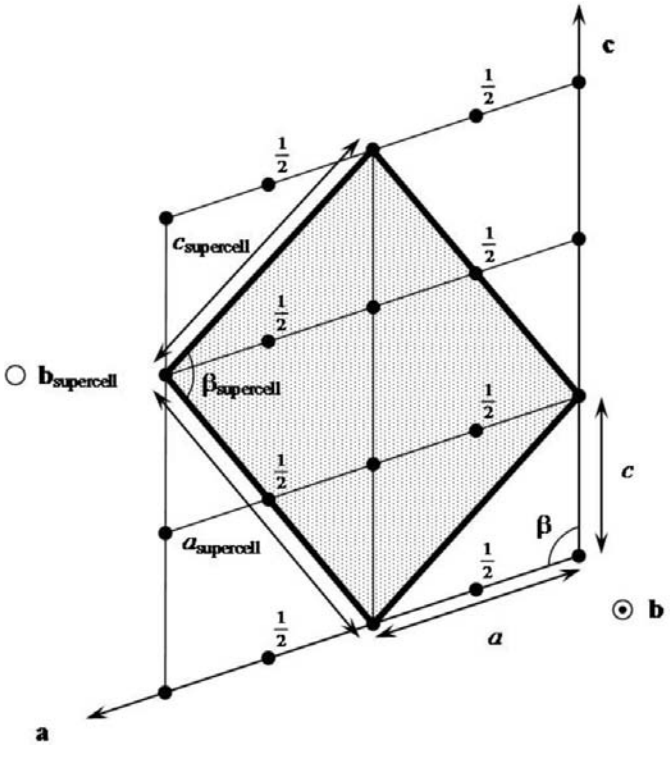

Figure 1
Identification of a supercell within the high-temperature β'-$Zn_2V_2O_7$-phase solid solution with unit-cell dimensions very similar to those quoted by Hng & Knowles (1999) for the phase designated γ-$Zn_3(VO_4)_2$, reported as a minor second phase in zinc oxide-based varistor materials doped with vanadium oxide and manganese oxide.

A search of the literature in the light of the work of Kurzawa *et al.* (2001) revealed Russian work on phase equilibria in the ZnO–MnO–V_2O_5 system (Zhuravlev *et al.*, 1993*a*,*b*; Surat *et al.*, 1996*a*,*b*; Krasnenko *et al.*, 2002*a*,*b*), in which a particular phase designated the *L* phase by Krasnenko and co-workers is reported to occur in the pseudobinary $Mn_2V_2O_7$–$Zn_2V_2O_7$ system. The *L* phase is reported to have a relatively wide composition range from 18.8 (± 1.3) to 53.8 (± 1.3) mol% $Mn_2V_2O_7$ within this pseudobinary system (Krasnenko *et al.*, 2002*a*,*b*). Krasnenko *et al.* (2002*a*,*b*) show that this phase has a characteristic Cu $K\alpha$ X-ray signature of two strong peaks close to one another at a 2θ value of 28°, with a third strong peak at a 2θ value of 29°. Zhuravlev *et al.* (1993*a*,*b*) report that this phase is a thortveitite-type phase having a monoclinic unit cell with $a = 13.342$, $b = 8.559$, $c = 9.976$ Å and $\beta = 105.81^\circ$ at a composition of 30 mol% $Mn_2V_2O_7$–70 mol% $Zn_2V_2O_7$, with the values of *a*, *b*, *c* and β varying very slightly across the composition range of the phase. The *a* and *c* parameters of the *L* phase reported by Zhuravlev and co-workers are in essence double those of the high-temperature β'-$Zn_2V_2O_7$ solid solution prototype thortveitite structure (Krasnenko *et al.*, 2003*a*,*b*), so that the proposed unit cell of the *L* phase has $Z = 8$ rather than $Z = 2$ for thortveitite (Zachariasen, 1930; Cruickshank *et al.*, 1962). No further details, such as the lattice type, space group or details of the crystal structure of the *L* phase are given in this Russian work.

It is apparent from the description of the phase designated γ-$Zn_3(VO_4)_2$ in zinc oxide varistor ceramics and the description of the *L* phase that there are notable similarities between the two phases, despite clear differences in their reported unit cells. The experimental (Zn + Mn):V ratio for the phase designated γ-$Zn_3(VO_4)_2$ would be consistent with a pyrovanadate in the pseudobinary $Mn_2V_2O_7$–$Zn_2V_2O_7$ system. Furthermore, the ratio of Zn:Mn would also fit the *L* phase. Both phases have a similar *b* lattice parameter and both phases have characteristic Cu $K\alpha$ X-ray diffraction peaks in the range 28—29° 2θ, just before the strong 100 ZnO peak at a 2θ value of 31.77° (ICDD PDF number 36-1451). The volume, *V*, of the unit cell of the *L* phase at a composition of 30 mol% $Mn_2V_2O_7$–70 mol% $Zn_2V_2O_7$ is 1096.1 Å^3, giving a *V*/*Z* value of 137.0 Å^3 for $Z = 8$ (Zhuravlev *et al.*, 1993*a*,*b*). By comparison, the unit-cell volume of the phase designated γ-$Zn_3(VO_4)_2$ is 833.4 Å^3, so that if there were six formula units per unit cell, *V*/*Z* would be 138.9 Å^3. In contrast to this, the high-temperature β'-$Zn_2V_2O_7$ phase solid solution with $Z = 2$ at the zinc pyrovanadate composition has a *V*/*Z* value of 139.8 Å^3 given the lattice parameters of $a = 6.9324$, $b = 8.4394$,

Table 1
Experimental data.

Crystal data	
Chemical formula	$Mn_{0.6}O_7V_2Zn_{1.4}$
M_r	338.37
Cell setting, space group	Monoclinic, $C2/m$
Temperature (K)	298
a, b, c (Å)	10.37908 (11), 8.55572 (9), 9.35394 (10)
β (°)	98.4667 (9)
V (Å^3)	821.58 (2)
Z	6
D_x (Mg m^{-3})	4.10
Radiation type	Cu $K\alpha$
Specimen form, colour	Flat sheet, black–brown
Specimen size (mm)	20 × 20 × 0.2
Specimen preparation pressure (kPa)	100
Specimen preparation temperature (K)	873–923
Data collection	
Diffractometer	Bruker D8
Data collection method	Powder on a flat mount; scan method $2\theta/\theta$
2θ (°)	$2\theta_{min}$ = 7.98641, $2\theta_{max}$ = 157.98042, increment = 0.018
Refinement	
Refinement on	I_{net}
R factors and goodness-of-fit	R_p = 0.076, R_{wp} = 0.099, R_{exp} = 0.075, S = 1.15
Wavelength of incident radiation (Å)	1.540562, 1.544390
Excluded region(s)	None
Profile function	Pseudo-Voigt
No. of parameters	53
$(\Delta/\sigma)_{max}$	0.001

Bruker AXS *TOPAS* (Coelho, 2003).

c = 5.0326 Å and β = 108.272° determined by Krasnenko *et al.* (2003*a*,*b*) for this $C2/m$ thortveitite structural type.

An examination of the unit-cell parameters and the Bravais lattices of β'-$Zn_2V_2O_7$ and the phase designated γ-$Zn_3(VO_4)_2$ shows that a monoclinic C Bravais lattice supercell can be identified within the β'-$Zn_2V_2O_7$ structure with Z = 6 and supercell dimensions strikingly similar to the values of a = 10.40, b = 8.59, c = 9.44 Å and β = 98.8° reported for γ-$Zn_3(VO_4)_2$ by Hng & Knowles (1999). This supercell, shown shaded in Fig. 1, has a = 10.2768, b = 8.4394, c = 9.7602 Å and β = 97.755°. The **b** axis of the supercell is antiparallel to the **b** axis of β'-$Zn_2V_2O_7$, so that the axes of the supercell form a right-handed set. It is apparent from Fig. 1 that the supercell can retain one third of the lattice points of the $C2/m$ thortveitite structural type – the two in the (001) plane of the supercell at z = 0.

It is therefore evident from these considerations that there are strong similarities between the characteristics of the L phase and the phase reported by Hng & Knowles (1999).

3. Experimental

3.1. Specimen preparation

High-purity powders of ZnO (Aldrich), V_2O_5 (Aldrich) and MnO (Aldrich) were used for the preparation of α-$Zn_2V_2O_7$ and α-$Mn_2V_2O_7$ powders. Powders of the appropriate chemical compositions were pressed into pellets and sintered either at 873 K for 48 h or 1073 K for 24 h on alumina substrates to achieve chemical homogeneity, subsequently confirmed by X-ray diffraction of powders produced from the crushed pellets. Chemical reaction between the V_2O_5 in the pellets and the alumina substrates occurred at 1073 K because of the existence of a eutectic at 931 K in the Al_2O_3–V_2O_5 binary phase diagram (Cheshnitskii *et al.*, 1983*a*,*b*); firing at 873 K prevented this undesired chemical reaction, but slowed down the kinetics of the desired chemical reactions in the pellets between either ZnO and V_2O_5 or MnO and V_2O_5, as appropriate.

Zinc-rich $(1-x)Zn_2V_2O_7$–$xMn_2V_2O_7$ compounds with x values of 0.05–0.30 in steps of 0.05 were obtained by mixing together appropriate quantities of α-$Zn_2V_2O_7$ and α-$Mn_2V_2O_7$ powders. Powders were pressed into pellets and then sintered at 873−923 K for 24 h on alumina substrates, after which they were reground into a powder. Owing to the very sluggish nature of the chemical reaction between α-$Zn_2V_2O_7$ and α-$Mn_2V_2O_7$ at these temperatures, this process was repeated up to ten times for each value of x in order to produce the desired equilibrium phase(s) at room temperature at each composition.

3.2. X-ray powder diffraction

Two types of experiments were undertaken, one type to confirm the form of the Zn-rich end of the $Zn_2V_2O_7$–$Mn_2V_2O_7$ phase diagram and establish the general characteristics of the X-ray powder diffraction pattern from the L phase, and the other to obtain good quality data for the composition $(Zn_{0.7}Mn_{0.3})_2V_2O_7$ for structural analysis (see Table 1).[1]

The X-ray data for structural analysis were collected in three separate, similar runs in a Bruker D8 in Bragg–Brentano geometry using Cu $K\alpha_{1,2}$ radiation, with primary and secondary Soller slits, a secondary beam monochromator, a 0.2 mm receiving slit and the scintillation counter in continuous mode with a step of 0.018° and total dwell time from the three runs of 36 s. The area of the sample in the beam was such that a divergence slit and related anti-scatter slit of 0.3° could be used to cover the 2θ range between 8 and 158° without over-illumination at the lowest angles of interest. The sample was rotated in the beam and fixed to the sample holder with a proprietary hairspray which did not affect the diffraction pattern obtained from the $(Zn_{0.7}Mn_{0.3})_2V_2O_7$ powder. This produced a dataset with 959 reflections used for structural analysis. At the lowest diffraction angles peaks had a width of ∼ 0.08° (Cu $K\alpha_1$), while at the highest accessible angles peaks were fitted with widths of ∼ 0.24° Cu $K\alpha_1$. Thus, with a monoclinic cell volume of ∼ 820 Å^3, most of the α_1 and α_2 reflections overlapped with other reflections, so that the number of truly independent observations was much less than 959 reflections, and instead close to 100.

[1] Supplementary data for this paper are available from the IUCr electronic archives (Reference: WH5004). Services for accessing these data are described at the back of the journal.

Using the data from electron diffraction, the stronger low-angle peaks were first indexed manually, after which a dataset up to $\sim 60^\circ$ was used to refine the cell parameters with a Le Bail (structure-free) fit. The final cell parameters came from the Rietveld refinement using the 959 reflections from 8 to 158° 2θ. Rietveld refinements (Rietveld, 1969; McCusker *et al.*, 1999) were undertaken using the Bruker AXS *TOPAS* Version 3 software (Coelho, 2003).

3.3. Electron microscopy

Scanning electron microscopy was used both to image the $(Zn_{0.7}Mn_{0.3})_2V_2O_7$ powder and to confirm the chemical composition of the powder by energy-dispersive X-ray (EDX) microanalysis. The microscope used was a JEOL JSM-5800LV scanning electron microscope. Suitable samples were prepared by depositing powder onto a piece of carbon adhesive, after which the non-carbon-coated sample was examined under a low vacuum condition in the microscope.

For transmission electron microscopy (TEM), suspensions of the $(Zn_{0.7}Mn_{0.3})_2V_2O_7$ powder in propan-2-ol solution were first deposited onto 300 mesh holey carbon copper grids (Agar). After carbon coating, samples were examined in a JEOL 200CX transmission electron microscope at an acceleration voltage of 200 kV.

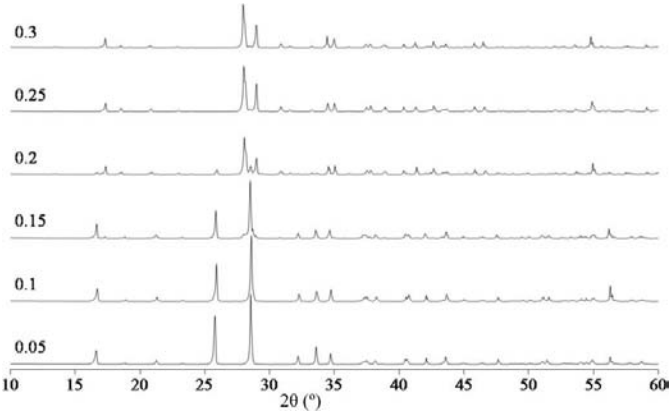

Figure 2
Powder X-ray diffraction patterns from the $Zn_2V_2O_7$–$Mn_2V_2O_7$ pseudobinary system for compositions of the general form $(Zn_{1-x}Mn_x)_2V_2O_7$. Values of x are shown on the left-hand side above each diffraction pattern. Peaks for $x = 0.05$ and 0.1 are from the α-$Zn_2V_2O_7$ solid solution in which manganese substitutes for zinc (Krasnenko *et al.*, 2002*a*,*b*). Peaks for $x = 0.25$ and 0.3 are from the pure L phase, while for $x = 0.15$ and 0.2 the peaks evident in the X-ray diffraction patterns are from both the α-$Zn_2V_2O_7$ solid solution and the L phase.

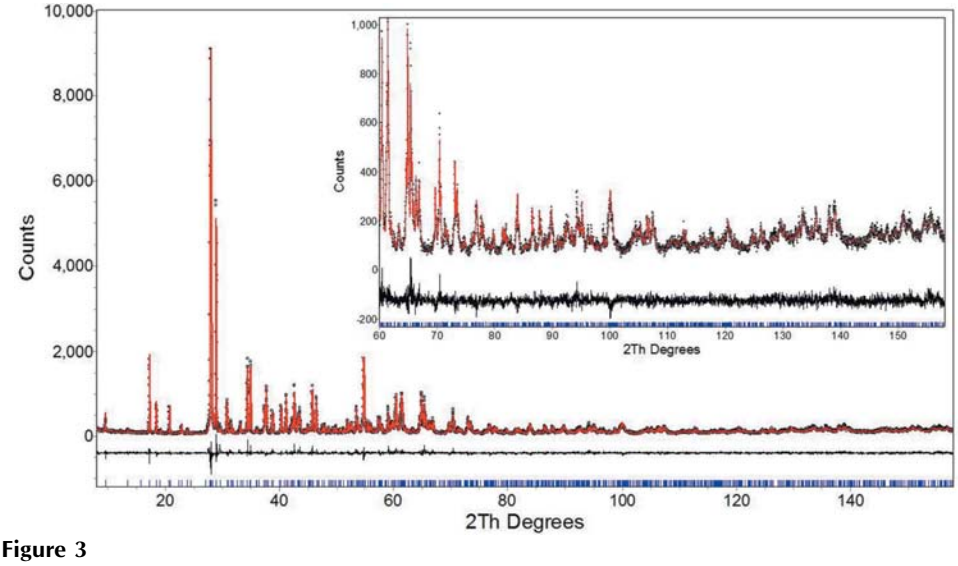

Figure 3
Observed (dotted) and calculated (solid line) X-ray powder diffraction pattern profiles for $(Zn_{0.7}Mn_{0.3})_2V_2O_7$ at room temperature, together with the difference profile.

4. Results and discussion

4.1. Phases at room temperature in the Zn-rich end of the $Zn_2V_2O_7$–$Mn_2V_2O_7$ pseudobinary system

Krasnenko *et al.* (2002*a*,*b*) report that α-$Zn_2V_2O_7$, the low-temperature polymorph of zinc pyrovanadate (ICDD PDF number 38-0251), can take up to 12.5 mol% $Mn_2V_2O_7$ into solid solution, while compositions with 15 and 17.5 mol% $Mn_2V_2O_7$ are mixtures of α-$Zn_2V_2O_7$ and L phase. These observations are consistent with the current work (Fig. 2), where the L phase is not detected in $(Zn_{1-x}Mn_x)_2V_2O_7$ powders when $x = 0.05$ and 0.1, but is detected when $x = 0.15$. The X-ray diffraction pattern for $x = 0.2$ is also a two-phase mixture, but it is apparent that this is extremely close to the phase boundary with the L phase, again in broad agreement with Krasnenko *et al.*'s (2002*a*,*b*) work. The X-ray diffraction patterns for $x = 0.25$ and 0.3 were the single-phase L phase, characterized by the very strong peaks at 2θ values around 28 and 29° for Cu $K\alpha$ radiation.

4.2. The *L*-phase unit cell

Chemical analysis of nominal $(Zn_{0.7}Mn_{0.3})_2V_2O_7$ powders showed that they were of the expected composition (Table 2). TEM further confirmed that the electron diffraction patterns from low index zones that could be obtained from these powders were identical to those reported for the phase designated γ-$Zn_3(VO_4)_2$ elsewhere (Hng & Knowles, 1999; Hng *et al.*, 2001; Pfeiffer & Knowles, 2004). This match further highlighted the predicted existence of a low index peak at a 2θ value of around 9.5° for Cu $K\alpha$ radiation, subsequently confirmed by the more detailed X-ray powder diffraction data obtained from $(Zn_{0.7}Mn_{0.3})_2V_2O_7$ powders for the structural analysis using the 2θ range of 8–158°.

Refinement of the unit-cell dimensions proposed by Hng & Knowles (1999) after initial

Table 2
Average chemical composition of nominal $(Zn_{0.7}Mn_{0.3})_2V_2O_7$ powders obtained by SEM/EDS analysis.

Element	Measured wt%	Measured at%	Ideal (target) at%
Zn	27.6 ± 2.1	13.0 ± 1.1	12.73
Mn	8.7 ± 1.2	4.8 ± 0.8	5.45
V	30.5 ± 0.9	18.4 ± 0.4	18.18
O	33.2 ± 0.4	63.8 ± 0.3	63.64

manual indexing of the X-ray diffraction data for $(Zn_{0.7}Mn_{0.3})_2V_2O_7$ (Fig. 3) gave values of a = 10.3791 (1), b = 8.5557 (1), c = 9.3539 (1) Å and β = 98.467 (1)°. Reflections were extinct when $h + k$ was odd. The existence of $h0l$ reflections for $h = 2n + 1$ precluded space groups Cc and $C2/c$, leaving $C2$, Cm and $C2/m$ as possible space groups allowed by the diffraction symmetry, just as for thortveitite, $Sc_2Si_2O_7$ (Cruickshank *et al.*, 1962).

A further check on these unit-cell dimensions was made by calculating the unit-cell dimensions of the incorrect $Z = 8$ unit cell proposed by Zhuravlev *et al.* (1993*a*,*b*) from these data. Simple geometry shows that this would have a = 13.3422, b = 8.5557, c = 9.9735 Å and β = 105.808°, values remarkably close to those quoted by Zhuravlev *et al.* (1993*a*,*b*).

4.3. Crystal structure refinement

The starting model used for crystal structure refinement was that for the high-temperature $C2/m$ β'-$Zn_2V_2O_7$ thortveitite-type phase determined by Krasnenko *et al.* (2003*a*,*b*), the structural parameters for which are shown in Table 3. To take account of the relationship between the unit cells of β'-$Zn_2V_2O_7$ and the L phase shown in Fig. 1, a 3 × 3 transformation matrix was constructed so that an atom at a vector position $[uvw]_{\beta'}$ becomes an atom at $[UVW]_L$, where

$$\begin{bmatrix} U \\ V \\ W \end{bmatrix}_L = \begin{bmatrix} -\frac{1}{3} & 0 & -\frac{1}{3} \\ 0 & -1 & 0 \\ \frac{2}{3} & 0 & \frac{1}{3} \end{bmatrix} \begin{bmatrix} u \\ v \\ w \end{bmatrix}_{\beta'}.$$

From this $C2/m$ starting model, the cell parameters from the Le Bail fit and a fixed displacement parameter, B, of 0.5 Å^2, the scale factor and background of a $1/x$ term together with a tenth-order Chebychev polynomial were first refined. Subsequently, the cell parameters, specimen displacement error and the peak profile parameters were refined. Pseudo-Voigt functions were used for the profiles with components for both crystallite size and microstrain. The atomic coordinates of the metal-atom positions were then refined, followed by the O-atom coordinates. Finally, the displacement parameters were refined by constraining them to be the same for each element, and also to be the same for Zn and Mn. The occupancy of each of the Zn and Mn ion positions was fixed as 0.7 Zn, 0.3 Mn in the L phase; subsequent refinements with ordering on the Zn and Mn sites made no significant improvement.

The starting model based on the β'-$Zn_2V_2O_7$ thortveitite-type structure could not account for several peaks. However, the reasonably good fit for the three strongest reflections of $22\bar{1}$ (27.92°), 310 (28.06°) and 003 (28.93°) confirmed that this was a suitable starting structure. Small displacements of the metal atoms, mostly in the z direction, were sufficient to correct the relative intensities of the low-angle peaks.

Table 3
Atom positions in β'-$Zn_2V_2O_7$ thortveitite determined by Krasnenko *et al.* (2003*a*,*b*).

Space group $C2/m$.

Atom	Position	x	y	z
Zn	4*h*	0	0.31577	0.5
V	4*i*	0.21736	0	0.9049
O1	2*a*	0	0	0
O2	8*j*	0.2151	0.1519	0.7085
O3	4*i*	0.4091	0	0.2050

Rietveld refinement in $C2/m$ of the 27 atomic position coordinates and B parameters (allowed to vary between 0 and 1 Å^2) reduced the GOF to 1.32, with R_p = 0.0758, R_{wp} = 0.0993 and R_{exp} = 0.0751. The refined atomic positions and B parameters are in the supplementary material. Adjusting the occupancies of the Zn1 and Zn2 sites so that Mn occupied preferentially either the 8*j* or 4*h* site did not improve the refinement, implying that there is no clear preference for ordering of Mn and Zn atoms on these sites. Artificially increasing the vanadium B parameter to 0.25 Å^2 increased R_{wp} to 0.0999 with very small adjustments in the atomic position coordinates and the B parameters of Zn, Mn and O. Without a lower bound of 0 Å^2, the vanadium B parameter became negative without any significant improvement in R_{wp}.

The Rietveld refinement was able to reproduce intensity satisfactorily in the low 2θ 001 and 110 reflections, and interatomic distances were reasonable (Table 4). The V—O—V 180° bond angles characteristic of thortveitite (Cruickshank *et al.*, 1962) were relaxed in the refined structure; while the bond angle V1—O1*b*—V1 remained 180°, V2—O1*a*—V3 was reduced to 149.13° in the L phase. The principal atomic displacements of the metals occurred for the z values of Zn, Mn1 and V2, with movements relative to the thortveitite of ∼ 0.4 Å. Projection of the crystal structure of the L phase onto the plane equivalent to the ab plane for thortveitite illustrates their similarity (Fig. 4).

R_{wp} is relatively high, just below 0.10, but within an acceptable range for refinements from laboratory X-ray data (McCusker *et al.*, 1999). However, the difference profile in Fig. 3 suggests the true space group of the L phase could be the lower symmetry $C2$ or Cm. Careful examination of the CBED patterns from [001], [100] and [102] (Hng, 1999; Hng *et al.*, 2001) confirmed that the symmetry was characteristic of point group m (Buxton *et al.*, 1976). Alternative possibilities of $2_R mm_R$ (for point group $2/m$) or m_R (for point group 2) are inconsistent with the CBED, and show the space group for the L phase is Cm, rather than $C2/m$.

Using Cm, rather than $C2/m$, for the L phase increases the refinable fractional coordinates to 57 and no longer constrains any of the V—O—V bond angles to be 180° since no O atom occupies a centre of symmetry. Rietveld refinement in Cm

Table 4
Interatomic distances (Å) and multiplicities for the refinement of the *L*-phase crystal structure in the space group *C*2/*m* in which the Mn and Zn ions randomly occupy the positions Zn,Mn1 and Zn,Mn2 in the ratio 0.7:0.3.

Zn,Mn1—O2*b*	2.035 (7)	× 1
Zn,Mn1—O2*a*	2.049 (8)	× 1
Zn,Mn1—O3*c*	2.068 (9)	× 1
Zn,Mn1—O2*c*	2.082 (7)	× 1
Zn,Mn1—O3*b*	2.130 (9)	× 1
Zn,Mn1—O3*a*	2.073 (8)	× 2
Zn,Mn1—O2*c*	2.094 (8)	× 2
Zn,Mn1—O2*a*	2.291 (6)	× 2
V1—O2*a*	1.677 (8)	× 2
V1—O3*c*	1.704 (14)	× 1
V1—O1*b*	1.749 (3)	× 1
V2—O2*b*	1.630 (8)	× 2
V2—O1*a*	1.887 (10)	× 1
V2—O3*b*	1.922 (13)	× 1
V2—O3*b*	2.028 (10)	× 1
V3—O1*a*	1.710 (10)	× 1
V3—O2*c*	1.722 (8)	× 2
V3—O3*a*	1.774 (12)	× 1

failed to improve the GOF significantly, and moreover the interatomic distances became unreasonable. This could arise because the total number of adjustable parameters for *Cm* is comparable with the number of independent observations, or the deviation from *C*2/*m* is subtle and dependent upon oxygen positions which do not strongly contribute to the diffracted X-ray intensity. The comments of Cruickshank *et al.* (1962) concerning structure determination of single-crystal thortveitite in *C*2/*m, Cm* and *C*2 are particularly apt in this respect. We therefore infer that any deviation from *C*2/*m* cannot be determined using the current X-ray powder diffractometer data. Unequivocal structure determination will require the analysis of single crystals of the *L* phase, higher resolution and intense synchrotron powder data, or neutron scattering that will be sensitive to the location of oxygen.

5. Conclusions

A reassessment of the crystal structure of the *L* phase, $(Zn_{1-x}Mn_x)_2V_2O_7$ ($0.188 < x < 0.538$), in the pseudobinary $Mn_2V_2O_7$–$Zn_2V_2O_7$ system shows that it has a monoclinic *C* lattice with structural parameters different from those previously reported. Structural refinement of X-ray powder diffractometer data in the space group *C*2/*m* shows that the *L* phase has a thortveitite-related structure whereby slight distortions of the prototype thortveitite structure produce a unit cell with $Z = 6$ rather than the $Z = 2$ of thortveitite. Attempts to refine further the crystal structure in the non-centrosymmetric point group *Cm* indicated by prior convergent-beam electron diffraction work were unsuccessful, implying that any structural deviation from the structure obtained in *C*2/*m* is very subtle and will require single-crystal work or powder data from a synchrotron or neutron source. We suggest that this thortveitite supercell structure may well occur in other multi-component systems in which relatively low-temperature phase transitions are allowed by virtue of the lack of stability on cooling of a higher-temperature thortveitite-type solid solution.

We would like to thank the Royal Society and the Indian National Science Academy for financial support for one of us (AS) through their joint international exchange programme. We would also like to thank Professor Simon A. T. Redfern of the Department of Earth Sciences, University of Cambridge, for undertaking an analysis of our data using the *GSAS* software and for helpful discussions about the feasibility of the successful refinement of X-ray laboratory powder diffraction data in non-centrosymmetric space groups.

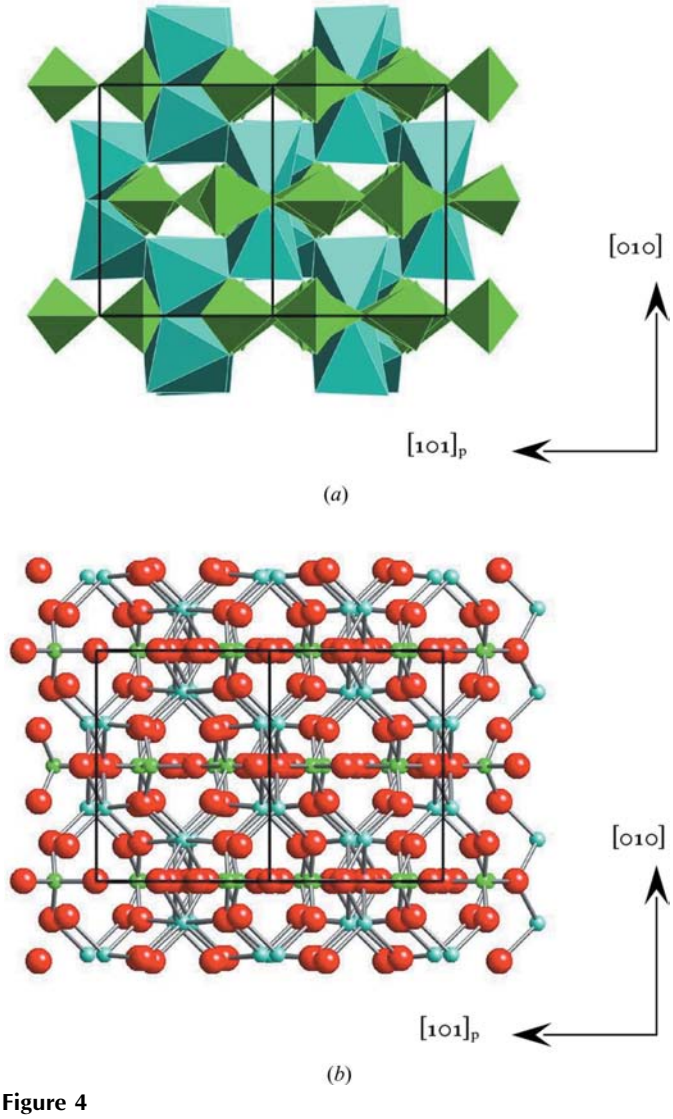

Figure 4
(*a*) Polyhedral model and (*b*) ball-and-stick model of the structure of the *L* phase viewed down the [$\bar{1}$01] direction, the direction equivalent to the [001] direction in the high-temperature β'-$Zn_2V_2O_7$ solid solution prototype thortveitite structure. In (*a*) the coordination polyhedra of the V atoms are green; those of the Zn and Mn atoms are light blue. In (*b*) O atoms are red, V atoms are green, and Zn and Mn atoms are light blue. The subscript *p* denotes the fact that the vector normal to [$\bar{1}$01] and [010] is the projection of [101]; [101] actually makes an angle of 96° with [101].

References

Brown, J. J. & Hummel, F. A. (1965). *Trans. Br. Ceram. Soc.* **64**, 419–437.

Buxton, B. F., Eades, J. A., Steeds, J. W. & Rackham, G. M. (1976). *Philos. Trans. R. Soc. London A*, **281**, 171–194.

Chen, C.-S. (2003). *J. Mater. Sci.* **38**, 1033–1038.

Cheshnitskii, S. M., Fotiev, A. A. & Surat, L. L. (1983*a*). *Zh. Neorg. Khim.* **28**, 1342–1344.

Cheshnitskii, S. M., Fotiev, A. A. & Surat, L. L. (1983*b*). *Russ. J. Inorg. Chem.* **28**, 758–759.

Coelho, A. A. (2003). *TOPAS User's Manual*, Version 3.0. Bruker AXS GmbH, Karlsruhe, Germany.

Cruickshank, D. W. J., Lynton, H. & Barclay, G. A. (1962). *Acta Cryst.* **15**, 491–498.

Gopal, R. & Calvo, C. (1971). *Can. J. Chem.* **49**, 3056–3059.

Hng, H.-H. (1999). PhD thesis. University of Cambridge, England.

Hng, H.-H. & Chan, P. L. (2002). *Mater. Chem. Phys.* **75**, 61–66.

Hng, H.-H. & Chan, P. L. (2004). *Ceram. Int.* **30**, 1647–1653.

Hng, H.-H. & Knowles, K. M. (1999). *J. Eur. Ceram. Soc.* **19**, 721–726.

Hng, H.-H. & Knowles, K. M. (2000). *J. Am. Ceram. Soc.* **83**, 2455–2462.

Hng, H.-H., Knowles, K. M. & Midgley, P. A. (2001). *J. Am. Ceram. Soc.* **84**, 435–441.

Krasnenko, T. I., Rotermel, M. V., Zolotukhina, L. V., Maksimova, L. G. & Zakharov, R. G. (2002*a*). *Zh. Neorg. Khim.* **47**, 1888–1891.

Krasnenko, T. I., Rotermel, M. V., Zolotukhina, L. V., Maksimova, L. G. & Zakharov, R. G. (2002*b*). *Russ. J. Inorg. Chem.* **47**, 1737–1740.

Krasnenko, T. I., Zubkov, V. G., Tyutyunnik, A. P., Zolotukhina, L. V. & Vasyutinskaya, E. F. (2003*a*). *Kristallografiya*, **48**, 40–43.

Krasnenko, T. I., Zubkov, V. G., Tyutyunnik, A. P., Zolotukhina, L. V. & Vasyutinskaya, E. F. (2003*b*). *Crystallogr. Rep.* **48**, 35–38.

Kuo, C.-T., Chen, C.-S. & Lin, I.-N. (1998). *J. Am. Ceram. Soc.* **81**, 2949–2956.

Kurzawa, M., Rychlowska-Himmel, I., Bosacka, M. & Blonska-Tabero, A. (2001). *J. Therm. Anal. Calorim.* **64**, 1113–1119.

McCusker, L. B., Von Dreele, R. B., Cox, D. E., Louër, D. & Scardi, P. (1999). *J. Appl. Cryst.* **32**, 36–50.

Nahm, C.-W. (2007*a*). *J. Mater. Sci.* **42**, 8370–8373.

Nahm, C.-W. (2007*b*). *Solid State Commun.* **143**, 453–456.

Nahm, C.-W. (2008*a*). *Mater. Sci. Eng. B*, **150**, 32–37.

Nahm, C.-W. (2008*b*). *J. Mater. Sci. Mater. Electron.* **19**, 1023–1029.

Pfeiffer, H. & Knowles, K. M. (2004). *J. Eur. Ceram. Soc.* **24**, 1199–1203.

Rietveld, H. M. (1969). *J. Appl. Cryst.* **2**, 65–71.

Surat, L. L., Zhuravlev, V. D., Fotiev, A. A. & Velikodnyi, Yu. A. (1996*a*). *Zh. Neorg. Khim.* **41**, 1370–1372.

Surat, L. L., Zhuravlev, V. D., Fotiev, A. A. & Velikodnyi, Yu. A. (1996*b*). *Russ. J. Inorg. Chem.* **41**, 1311–1313.

Zachariasen, W. H. (1930). *Z. Kristallogr.* **73**, 1−6.

Zhuravlev, V. D., Velikodnyi, Yu. A. & Surat, L. L. (1993*a*). *Zh. Neorg. Khim.* **38**, 1221–1224.

Zhuravlev, V. D., Velikodnyi, Yu. A. & Surat, L. L. (1993*b*). *Russ. J. Inorg. Chem.* **38**, 1133-1136.